Effect of atomic reagent approach geometry on reactivity: Reactions of aligned Ca($^1P_1$) with HCl, Cl_2, and CCl_4

Charles T. Rettner and Richard N. Zare

Department of Chemistry, Stanford University, Stanford, California 94305
(Received 12 April 1982; accepted 18 May 1982)

The reactivity of Ca($^1P_1$) with HCl, Cl_2, and CCl_4 has been studied as a function of Ca($^1P_1$) alignment with respect to the initial average relative velocity vector of the reagents in a beam-gas scattering geometry. While the total chemiluminescence cross section for the Ca($^1P_1$) + HCl reaction is insensitive to Ca($^1P_1$) alignment, the branching into the CaCl($A\,^2\Pi$) and CaCl($B\,^2\Sigma^+$) states depends markedly on the approach direction of the atomic p orbital. Parallel approach of the Ca p orbital favors CaCl($B\,^2\Sigma^+$) formation while perpendicular approach favors CaCl($A\,^2\Pi$). A weak dependence of these effects on CaCl($B\,^2\Sigma^+$) vibrational state is observed. The analogous reaction with Cl_2 shows a strong preference for perpendicular p-orbital approach in both chemiluminescent product channels, which is most prominant for the CaCl($A\,^2\Pi$) state. In contrast, the reaction with CCl_4 displays no significant dependence on approach geometry. For Ca($^1P_1$) + Cl_2, a chemi-ionization channel is observed, showing a preference for perpendicular alignment intermediate between that for the CaCl($A\,^2\Pi$) and CaCl($B\,^2\Sigma^+$) channels. Chemiluminescence spectra, absolute chemiluminescence cross sections, branching ratios, and emission polarizations are also presented. Results are interpreted in terms of an electron-jump model in which the symmetry of the reagents is preserved during a reactive encounter.

I. INTRODUCTION

It has long been accepted that chemical reactivity depends markedly on reagent approach geometry. Thus geometric factors are invariably included when accounting for or predicting reactivities. For example, bimolecular rates are traditionally viewed as scaling with a so-called "steric factor"[1] while reagent orientation plays a central role in frontier orbital theories[2,3] of chemical reactivity. However, the direct interrogation of reactive geometric requirements is difficult and only relatively few such studies have been carried out to date, all employing molecular beam conditions to control the *direction* of approach.

Reagents can be oriented or aligned with respect to the approach direction. If the spatial distribution of reagents is isotropic, then the magnetic sublevels M (defined with respect to the approach direction as the quantization axis) are equally populated. Orientation implies that $+M$ and $-M$ sublevels are unequally populated so that the reagent has a preferred direction; alignment implies that $+M$ and $-M$ sublevels are equally populated but populations differ between $|M|$ levels. Thus, oriented reagents may be considered as single-headed arrows in flight while aligned reagents may be regarded as double-headed arrows in flight.

The effect of reagent approach geometry on chemical reactions has been studied using only two techniques for reagent preparation. Most studies have employed external fields to prepare oriented polar symmetric top molecules.[4] Notable examples are the reactions of alkali atoms with oriented CH_3I[5–12] and CF_3I,[6,13,14] and the reaction of O_3 with oriented NO.[15] As expected, large reactive asymmetries are observed. Thus for Rb + CH_3I there is a substantial cone of approach at the CH_3- end for which no reaction occurs,[12] while K + CF_3I exhibits (dynamically distinct) reactivity at both ends.[13,14] In the O_3 + NO study it was found that the reaction proceeds preferentially via the N- end.[15] However, even in the best circumstances, external field orientation often provides a poor degree of spatial control, whose exact characterization presents difficulties.

Laser photoselection represents the only other reagent pointing technique employed so far. In this approach a polarized light beam serves to produce substantially aligned populations, as first suggested by Kastler.[16] Optical pumping[17] and photodissociation[18,19] (including predissociation) can be used to prepare anisotropic distributions of ground state species, while absorption naturally produces aligned excited-state populations.[20] Such techniques are not restricted to polar species. Thus Estler and Zare[21] sought to examine the reactive asymmetry of the $I_2(B\,^3\Pi_{0^+_u})$ + In, Tl reaction systems while Rothe *et al.*[22] determined that Na_2^+ ions are preferentially dissociated when the reagent approach direction is perpendicular to the plane of rotation. In another study, Karny *et al.*[23] observed that the alignment of HF($v = 1$) influences the quantum state distribution of SrF product following reaction with Sr atoms. More recently we have carried out the first studies involving aligned *atomic* species.[24] We investigated the influence of the alignment of laser-excited Ca($^1P_1$) reagent on the outcome of the chemiluminescent reaction

$$\mathrm{Ca}(^1P_1) + \mathrm{HCl} \rightarrow \mathrm{CaCl}(A\,^2\Pi, B\,^2\Sigma^+) + \mathrm{H}\ . \qquad (1)$$

The chemiluminescent reactions of Ca($^1P_1$) atoms were considered particularly well suited to such studies for several reasons. The calcium atom is excited via the $^1S_0$–$^1P_1$ transition of 422.7 nm, making possible almost total alignment of the $4p$ orbital of Ca using visible dye laser excitation. Furthermore, the polarization of the resonance radiation emitted by the Ca($^1P_1$) atom is readily determined, providing a direct measure of the degree of alignment. Chemiluminescent products can be sensitively detected and resolution of the chemiluminescence spectrum provides information about the product state distribution. The HCl reagent was chosen for these initial investigations for two further reasons. First the reaction

 0021-9606/82/172416-14$02.10

$$Ca(^1S_0) + HCl - CaCl(X\,^2\Sigma^+) + H \quad (2)$$

is substantially endothermic; hence interference by laser-induced fluorescence from the ground-state $CaCl(X\,^2\Sigma^+)$ product[25] is not expected. Second, the analogous chemiluminescent reaction of $Ca(^1D_2)$ + HCl is well known,[26–28] giving us confidence that the chemiluminescence spectrum from Reaction (1) could be readily assigned.

While the total chemiluminescence cross section for Reaction (1) was found to be relatively insensitive to atomic alignment, the branching ratio into the two CaCl* states was observed to depend quite strongly on the approach geometry.[24] In this paper, we report more detailed data on the reactive asymmetry of Reaction (1) as well as the chemiluminescence spectrum, product rotational polarization, and absolute chemiluminescence cross section. We also present similar data for two new reactions, those of $Ca(^1P_1)$ with Cl_2 and CCl_4. The reaction with Cl_2 shows a large reactive asymmetry and in contrast to that with HCl the total chemiluminescent cross section is seen to depend strongly on the approach geometry. The reaction with CCl_4 does not appear to be influenced appreciably by the $Ca(^1P_1)$ approach geometry. In the case of Cl_2 alone, a chemi-ionization channel is observed. This also displays a marked geometric preference.

We suggest that our findings can be interpreted qualitatively using three simple principles: (1) the correlation of atomic orbitals in the $Ca(^1P_1)$ reagent with molecular orbitals in the $CaCl(A\,^2\Pi, B\,^2\Sigma^+)$ products, (2) the electron-jump model in which the covalent potential curve of the approaching reagents is crossed by various ionic curves, and (3) "orbital following" in which the orbital geometry is preserved as the reagents approach (adiabatic behavior).

II. EXPERIMENTAL

A. General

A global description of the apparatus and methodology will be outlined below while details of the atomic alignment technique and measurements of the alignment effects are considered within Sec. II B. All measurements are made under beam-gas conditions, whereby a beam of ground state calcium atoms is laser-pumped at the $Ca\ ^1S_0 - ^1P_1$ transition frequency in the presence of the reagent gas. A schematic of the apparatus is given in Fig. 1.

The scattering chamber and metal oven assembly have been described in detail previously.[25] Briefly, the calcium beam effuses from a 1 mm diameter, 1 mm long orifice in a 100 cm^3 capacity oven held at a temperature of 1075 K and located at a distance of 8 cm from the laser excitation zone. The graphite ovens used previously for indium[25] could not be opened after exposure to Ca under these conditions; consequently stainless steel ovens are used instead. These are sealed at their top end by compressing a 1 mm thick copper disk above a 0.125 mm thick molybdenum disk against a 0.3 mm high, 1.0 mm wide rounded knife edge. The

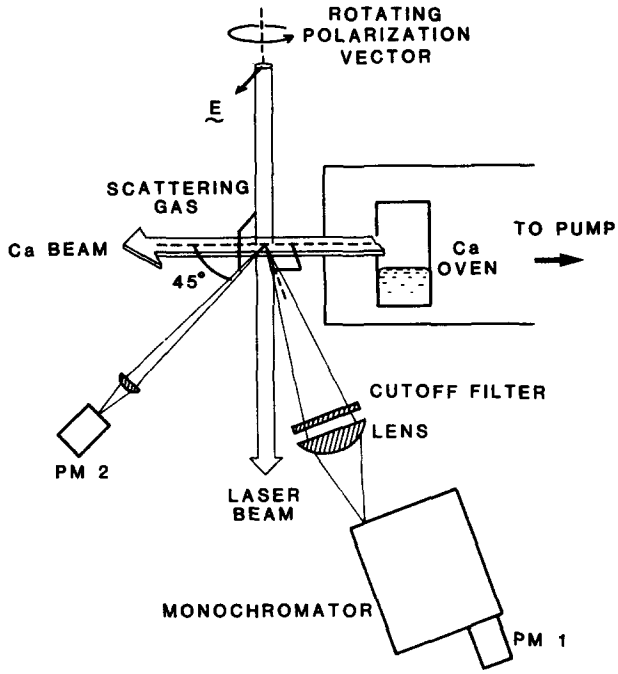

FIG. 1. Apparatus for determining the variation of laser-induced chemiluminsecence with the direction of the electric vector of the laser. Calcium atoms are prepared in the $4s\,4p\,^1P_1$ state with a known alignment with respect to the atomic beam.

rectangular beam (5 mm wide and 10 mm long) is collimated by a single slit placed 2 cm from the laser excitation zone. A molybdenum wire loop is placed 5 mm from the nozzle on the beam axis. Biasing this loop 20 V positive with respect to the oven body permits a metastable discharge to be run. This produces $Ca(^3P_{2,1,0})$ and $(^1D_2)$ atoms of which the $Ca(^1D_2)$ species are energetic enough to produce chemiluminescence from reaction with HCl, for comparison with the laser-pumped $Ca(^1P_1)$ reaction.

Scattering gases are added via a precision monel leak valve (Granville–Phillips Model 203-015) to pressures of $\sim 10^{-4}$ Torr as measured on an ionization gauge calibrated against a capacitance manometer. HCl (nominal purity, 99.99%) and Cl_2 (nominal purity, 99.5%) are used directly as received from Matheson Gas Products. The CCl_4 (J. T. Baker, spectral grade) is purified by repeated freeze–thaw cycles under vacuum.

Laser-induced chemiluminescence is viewed at right angles to the laser and atomic beams and collected by a 15 cm focal length lens. A cutoff filter placed in front of this lens limits transmission to the red of 440 nm. A screen restricts the lens aperture to a 5 cm diameter circle, amounting to a solid angle of 3×10^{-2} sr (0.25% collection efficiency). The chemiluminescence is imaged onto the slits of a 1 m monochromator (Interactive Technology) fitted with a 1200 grooves/mm grating blazed at 500 nm. Ultimate optical detection is on a cooled (Centronics, extended S-20 photocathode) photomultiplier (PM 1). Its output feeds either a fast picoammeter (Keithley 427) or a photon counting system,

as shown in Fig. 2.

In separate experiments, chemi-ions are monitored by positioning two 1 cm square copper plates 1 cm apart on either side of the laser excitation zone. A 90 V battery and the picoammeter complete a simple circuit.

An additional photomultiplier (PM 2) is placed at 45° to the metal beam axis and at 90° to the laser beam (Figs. 1 and 2). Atomic fluorescence is imaged by a 2.5 cm focal length, 1 cm aperture lens onto its photocathode via a 1 mm pinhole. This permits both the concentration and the polarization (see Sec. II C) of $Ca(^1P_1)$ atoms to be monitored.

B. Determination of alignment dependence

Aligned $Ca(^1P_1)$ atoms are readily obtained following absorption of polarized light at 422.7 nm. In these studies a linearly polarized dye laser is used to prepare the $Ca(^1P_1)$ atoms with their p orbital aligned along the electric vector **E** of the laser beam. Rotation of **E** therefore permits selection of p-orbital alignment in the laboratory. Figure 3 presents a schematic of the optical components used in this study.

A multimode home-built linear dye laser is employed, the components of which have been described elsewhere.[29] This has a conventional astigmatic three-mirror cavity[30] with a three-plate birefringent filter (Coherent) as well as an optional single etalon. The birefringent filter permits broadband tuning with a bandwidth ~1 cm^{-1}. Insertion of the ~1.5 cm^{-1} free spectral range etalon reduces this to ~0.1 cm^{-1}. Using stilbene 420 dye (Exciton) pumped with the 3 W UV output of an argon ion laser (Coherent CR12) maximum powers of ~300 mW are obtained at 422.7 nm with the birefringent filter alone, falling to ~200 mW with the etalon in place.

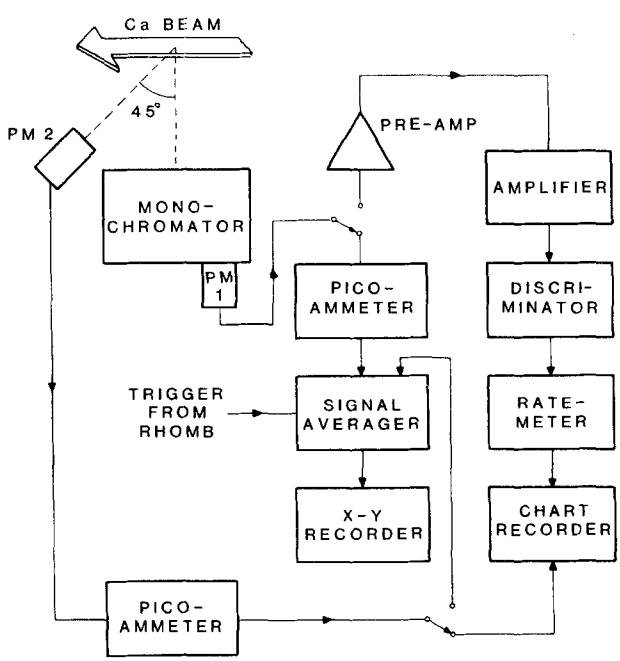

FIG. 2. Block diagram of the signal processing system.

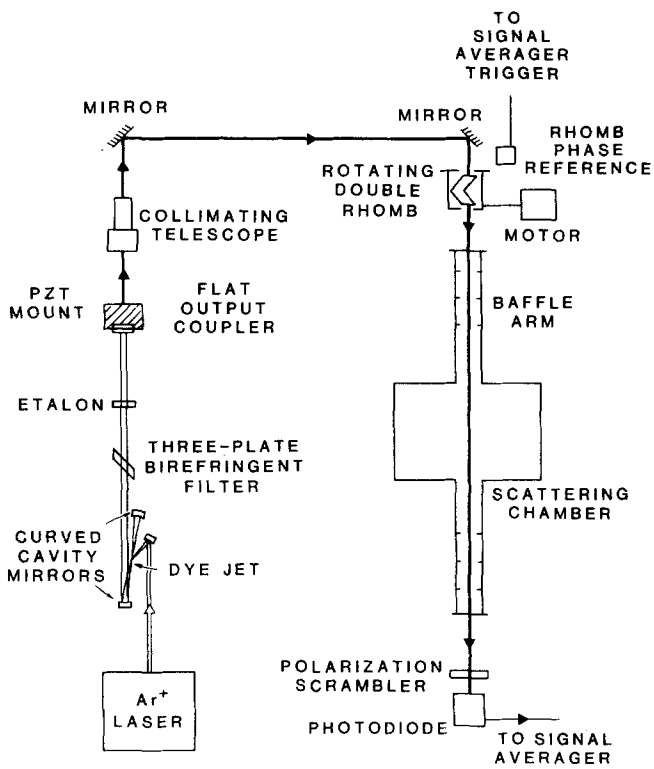

FIG. 3. Laser and optics. The linearly polarized dye laser output is directed vertically through the scattering chamber. A rotating double Fresnel rhomb causes the laser electric vector to spin.

The output coupler of this dye laser is mounted on a piezoelectric translation (Lansing Model 21.938) connected to a 115 V, 60 Hz supply. This greatly reduces noise by forcing the frequency of the laser modes to vary rapidly across the gain profile. Without this provision, random mode hopping causes fluctuations in the $Ca(^1P_1)$ population. A telescope collimates the laser output and a total of three 45° aluminum mirrors are used to direct the beam vertically through the scattering chamber.

The electric vector of the linearly polarized beam is rotated by passage through two optically contacted back-to-back Fresnel rhombs. This is shown in Fig. 4. By rotation of this assembly at 2.5 Hz, the **E** vector is caused to spin at four times this frequency. A phase reference is obtained from a photodiode placed above a disc that spins with the assembly. Light from a 6 V bulb passes through a 1 mm hole in this disc once each revolution, providing a 5 V, 0.5° wide reference pulse. In addition, a ~1 cm wide flag attached to the assembly blocks the laser once each revolution. This provides "laser off" signals for comparison with the effect of **E** vector rotation. Alignment of the assembly is critical. If the beam does not pass perpendicular to the plane of rotation, it will orbit its original direction once each revolution. Fortunately, effects due to such misalignments occur at one-fourth of the frequency of the **E** vector rotation and are therefore easily distinguished.

After the laser beam emerges from the rhomb assembly it only passes through a single perpendicular quartz window prior to crossing the atomic calcium

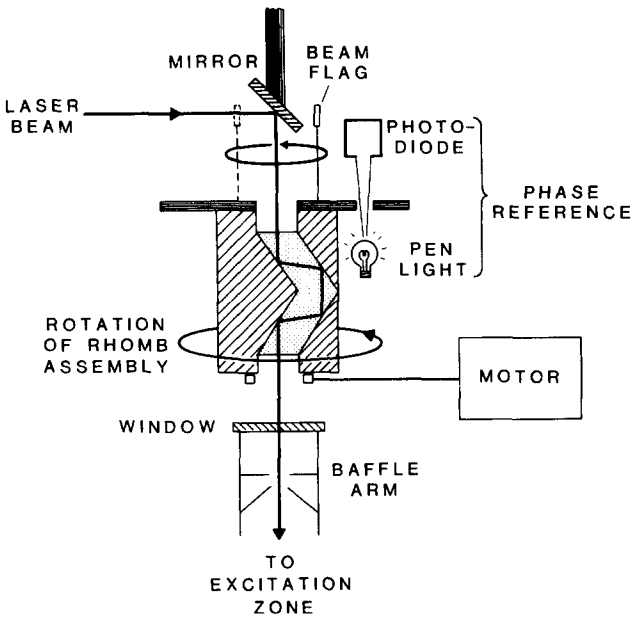

FIG. 4. Fresnel rhomb assembly for rotating the electric vector of the linearly polarized laser beam. As the assembly turns, the electric vector rotates four times as fast. Once each revolution, a beam flag intercepts the laser to provide "laser blocked" signals, while phase reference pulses are obtained from a penlight which illuminates a photodiode.

beam. In the excitation zone, the laser is $\gtrsim 98\%$ polarized and has a diameter of ~5 mm. Care is taken to ensure a good TEM_{00} mode, azimuthal symmetry being particularly important. This is necessary because the rhombs also cause the *profile* of the beam to rotate, but again at only one quarter of the **E** vector rate.

By feeding signals to a signal averager (Nicolet 1170 with 171/2 plug-in) whose sweeps are triggered by the rhomb assembly reference pulse, the effects of laser **E** vector rotation on various signals can be sensitively determined. It is important to check that the laser *power* does not vary as the rhombs rotate. This is accomplished by monitoring the beam with a photodiode placed behind a polarization scrambler (Karl Lambrecht) as it exits from the apparatus. A null effect is indicated by the recording of a flat trace on the signal averager. Signals in general, such as those from the laser-induced chemiluminescence, produce a trace with regular oscillations, the phase and amplitude of which reflect its **E** vector dependence. Hard copies of all data are obtained by output to an X-Y recorder.

C. Preparation of $Ca(^1P_1)$

All signals, atomic fluorescence, laser-induced chemiluminescence, and chemi-ionization, are found to increase linearly with laser power up to the maximum intensity employed of ~100 mW cm^{-2} GHz^{-1}. The $Ca(^1P_1)$ alignment is not sensitive to laser power under these conditions. Signals also increase with Ca beam density, but optical trapping of resonant radiation limits beam densities to $\lesssim 10^{11}$ atoms cm^{-3}. In all cases, tuning the laser off the atomic Ca $^1S_0$–$^1P_1$ line is found to be equivalent to blocking the laser beam. Thus, processes involving absorption of laser light by species other than $Ca(^1S_0)$ can be assumed to be negligible. In particular, there are no significant contributions from laser-induced fluorescence from ground state products.[25]

The $Ca(^1P_1)$ state lies 1802 cm^{-1} above the metastable $Ca(^1D_2)$ state, which may therefore be populated by radiative cascade. Simplistic steady-state kinetics suggest that

$$N(^1D_2)/N(^1P_1) = A(^1D_2{-}^1P_1)/F\ , \tag{3}$$

where $N(^1D_2)$ and $N(^1P_1)$ represent the populations of the $^1D_2$ and $^1P_1$ states, $A(^1D_2{-}^1P_1)$ is the transition probability for the Ca $^1D_2$–$^1P_1$ transition and F is the $Ca(^1D_2)$ fly-out rate.[25] $A(^1D_2{-}^1P_1)$ has been calculated[31] as 2.4×10^3 s^{-1}. For an effusive Ca beam crossed by a 2.5 mm radius laser we estimate $F \simeq 4\times10^5$ s^{-1}, giving $N(^1D_2)/N(^1P_1) \sim 0.6\%$. Direct observation of the electric quadrupole transition Ca $^1S_0$–$^1D_2$ at 457.5 nm revealed a fluoresence intensity $\sim 5\times10^{-9}$ of that observed for the Ca $^1S_0$–$^1P_1$ transition. Allowing for the differing transition probabilities, $A(^1S_0{-}^1D_2) \simeq 81$ s^{-1} [31] and $A(^1S_0{-}^1P_1) \simeq 2\times10^8$ s^{-1},[32] we obtain $N(^1D_2)/N(^1P_1) \simeq 1.2\%$. Much larger ratios would be obtained if the excitation zone occurs upstream of the observation zone. Finally, we note that $Ca(^3P_1)$ could not be detected via the spin forbidden Ca $^1S_0$–$^3P_1$ transition at 657.4 nm, even though $A(^1S_0{-}^3P_1) \simeq 3.9\times10^3$.[31] This suggests that $N(^3P_1)/N(^1P_1) \lesssim 10^{-6}$ and its presence can be neglected. Furthermore, since $Ca(^1D_2)$ and $Ca(^1P_1)$ have comparable chemiluminescence cross sections (see Sec. III A) the $Ca(^1D_2)$ makes a negligible contribution to the processes studied.

III. RESULTS

A. $Ca(^1P_1)$ + HCl

1. Chemiluminescence spectra

Figure 5 shows the laser-induced chemiluminescence spectrum obtained by illuminating the calcium beam at 422.7 nm in the presence of 3×10^{-4} Torr of HCl gas. This spectrum was recorded at a resolution of 0.4 nm and has been corrected for the wavelength response of the detection system, measured using an NBS standard lamp (Optronics, 245C). To minimize polarization ef-

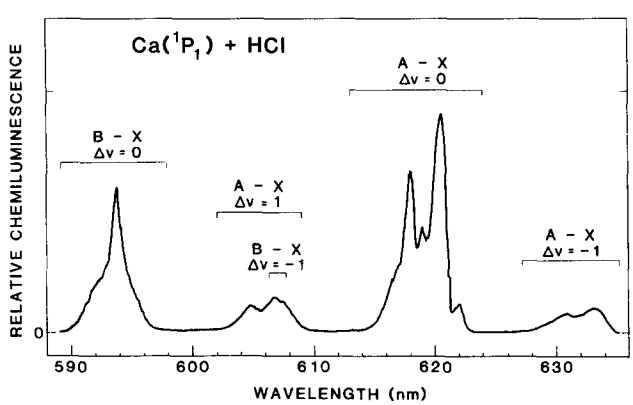

FIG. 5. Laser-induced chemiluminescence spectrum obtained by preparing $Ca(^1P_1)$ in a beam impinging on HCl gas.

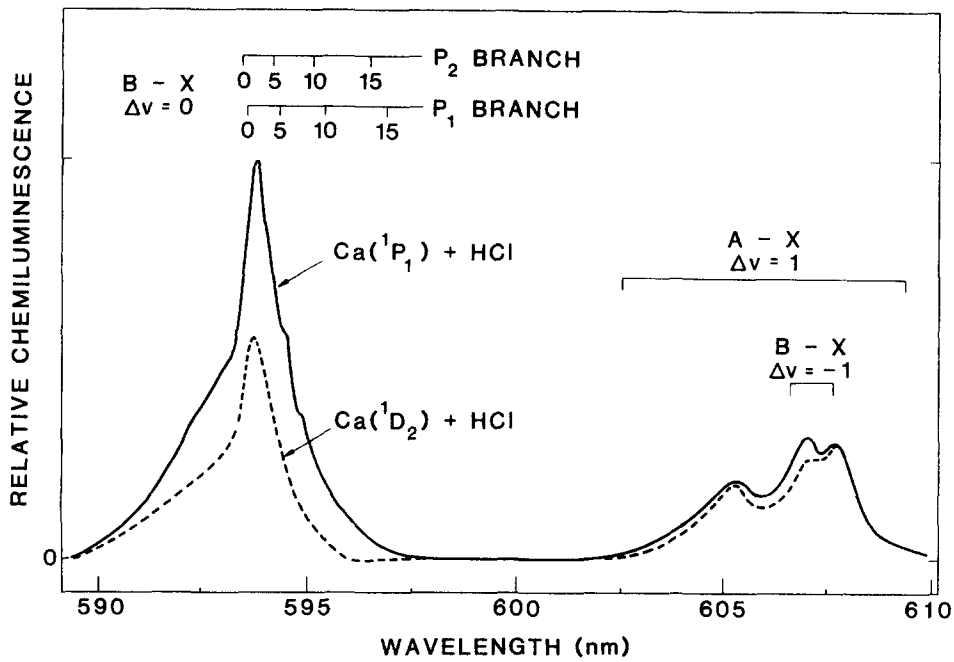

FIG. 6. Detailed comparison of the chemiluminescence spectra from the reactions of $Ca(^1P_1)$ (solid line) and $Ca(^1D_2)$ (dashed line) with HCl. Both spectra have been normalized to common relative intensities for their A-X $\Delta v = 0$ sequences (not shown).

fects, spectra were recorded with the E vector of the laser spinning and with a polarization scrambler in front of the entrance slit of the monochromator. The large peak at ~620.5 nm corresponds to $\sim 10^3$ counts s^{-1}. This peak and its neighboring peak at 618.0 nm are assigned to the $A\,^2\Pi_{1/2}$–$X\,^2\Sigma^+$ and the $A\,^2\Pi_{3/2}$–$X\,^2\Sigma^+$ subbands of the $\Delta v = 0$ sequence, respectively. The only other prominent feature in this spectrum, at 593.7 nm, is assigned to the $\Delta v = 0$ sequence of the $B\,^2\Sigma^+$–$X\,^2\Sigma^+$ band system.

The $Ca(^1P_1)$ + HCl chemiluminescence spectrum has not been reported previously. This spectrum strongly resembles that obtained from the reaction of $Ca(^1D_2)$ with HCl.[26–28] However, when the latter reaction is run in our apparatus under essentially identical conditions, we observe two notable differences. First, we find an approximately twofold increase in the B-X emission relative to the A-X emission in the case of the $Ca(^1P_1)$ reagent. Second, the B-X $\Delta v = 0$ sequence extends somewhat further to the red for the $Ca(^1P_1)$ reagent, indicating a higher degree of vibrational excitation. These differences are apparent from Fig. 6 which displays the chemiluminescence spectra obtained for the two reactions in the region of the CaCl B-X band system. The A-X systems for these two reagents have a more similar appearance. Both curves in Fig. 6 have been normalized to a common A-X relative intensity. The solid curve refers to the $Ca(^1P_1)$ reaction while the dashed curve refers to that for $Ca(^1D_2)$. It would seem that the feature located between 602 and 610 nm belongs largely to the A-X $\Delta v = 1$ sequence, since both reactions give nominally the same intensity in this band. However, a small shoulder at ~607 nm appears to belong to the B-X $\Delta v = -1$ sequence, being considerably enhanced in the $Ca(^1P_1)$ case.

From Figs. 5 and 6 we can obtain estimates for the branching ratio for production of CaCl (A) and (B) states, $\sigma(A)/\sigma(B)$. For the $Ca(^1P_1)$ and $(^1D_2)$ reactions, we obtain $\sigma(A)/\sigma(B) = 2.5 \pm 0.1$ and 4.4 ± 0.2, respectively. This latter value compares with a ratio of 4 ± 1 obtained by Telle and Brinkmann[27] based on the $\Delta v = 0$ sequence alone. Thus we see that the $Ca(^1P_1)$ reaction produces proportionally more $B^2\Sigma^+$ state than the $Ca(^1D_2)$ reaction. This trend is consistent with statistical partitioning of electronic energy. Using the result[33,34]

$$x_i \propto g_i (E_{\text{tot}} - E_i)^{5/2} , \tag{4}$$

where x_i is the fraction of trajectories producing the ith electronic state of electronic degeneracy g_i and E_{tot} is the total available energy, we obtain: $\sigma(A)/\sigma(B) = 2.7$ and 3.1 for the $Ca(^1P_1)$ and $Ca(^1D_2)$ reactions with HCl, respectively. Considering the rigid rotor harmonic oscillator assumptions made in deriving Eq. (4), these are in good agreement with the experimental values. In particular, the $\sigma(A)/\sigma(B)$ ratio for the $Ca(^1P_1)$ reaction is almost within the uncertainty of the measurement.

As noted above, it is apparent from Fig. 6 that the $Ca(^1P_1)$ reaction produces a noticeably broader B-X band, extending about 1.5 nm to the red. We interpret this as being due to the production of higher vibrational levels in this case. More precisely, the $Ca(^1P_1)$ reaction yields a $v'_{\max}$ of $\sim 16 \pm 1$ compared to 11 ± 1 for the $Ca(^1D_2)$ reaction. The uncertainty stems from the difficulty in estimating this quantity from an unresolved spectrum. Telle and Brinkmann[27] report $v'_{\max} = 12$ for the $Ca(^1D_2)$ reaction, which is likely to be accurate, since a higher resolution spectrum was employed. The differences in the $v'_{\max}$ values determined here correspond to ~22 kJ mol^{-1} more vibrational energy, which should be compared to the $Ca(^1P_1)$–$Ca(^1D_2)$ energy separation of 21.5 kJ mol^{-1}. Clearly, this entire difference in electronic excitation of the reagents can finds its way into vibrational excitation of products.

For the $Ca(^1P_1)$ + HCl system, we note that no signals are obtained in the 550–650 nm region with either the

laser blocked or tuned off the Ca $^1S_0$–$^1P_1$ transition. Similarly, no spectrum is obtained in the absence of HCl gas. The chemiluminescence increases linearly with HCl pressure below $\sim 1\times10^{-4}$ Torr, showing a characteristic "tailing off" due to attenuation of the Ca beam as pressures are raised.[27] However, the working pressure of 3×10^{-4} Torr is about a factor of 4 below the maximum in the signal versus pressure plot. Only the results of single-collision events can be observed under such conditions.[26,27] This is in accord with the fact that the radiative rates of the CaCl(A, B) states[35] are $\sim 10^8$ s^{-1} whereas quenching and fly-out rates are estimated to be $\lesssim 10^6$ s^{-1} and $\lesssim 10^5$ s^{-1}, respectively. Thus Figs. 5 and 6 represent spectra of nascent products.

2. Dependence on reagent alignment

Figure 7 displays various signals obtained as a function of the rhomb assembly angle. These were all recorded with the signal averager under identical conditions but with the monochromator set to select different wavelengths. In addition, trace (e) shows the baseline found in the absence of HCl. Each of the chemiluminescence traces (a)–(d) touch this baseline at the point where the laser is blocked, as described in Sec. II B. These results complement those presented previously (Fig. 1 of Ref. 24) which were recorded at the peak of the $\Delta v = 0$ sequences of the $A\,^2\Pi_{1/2}$–$X\,^2\Sigma^+$ and

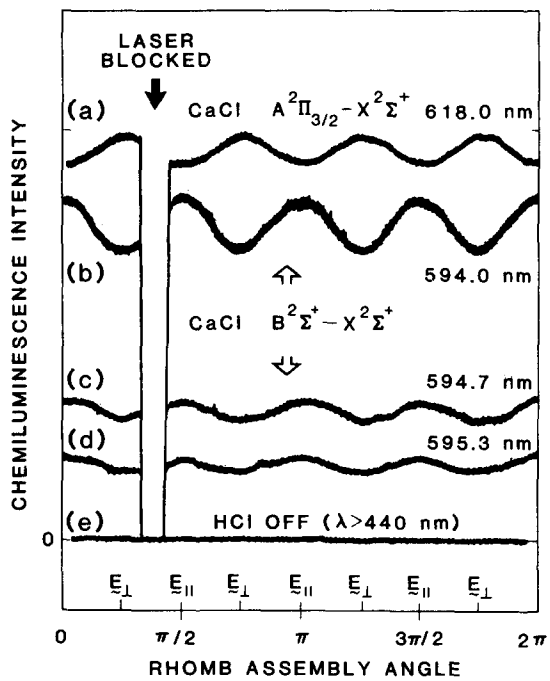

FIG. 7. Variation with rhomb assembly angle of chemiluminescence intensity for the reaction of Ca ($^1P_1$) with HCl. Trace (a) was recorded at the peak of the CaCl $A\,^2\Pi_{3/2}$–$X\,^2\Sigma^+$ system, while traces (b) to (d) refer to increasing vibrational excitation in the CaCl $B\,^2\Sigma^+$ state. Trace (e) was recorded in the absence of HCl gas. $E_\parallel$ and $E_\perp$ denote the positions where the electric vector of the laser is pointed parallel to and perpendicular to the average relative velocity vector of the reagents, respectively. Notice that all signals fall to the baseline as the laser is blocked.

TABLE I. Reagent alignment sensitivity factors at various wavelengths for the chemiluminescent reaction Ca ($^1P_1$) + HCl.

λ (nm)	Excited state	Lower limit for v'	S
620.5	$A\,^2\Pi_{1/2}$	...	-0.034 ± 0.005
618.0	$A\,^2\Pi_{3/2}$	...	-0.030 ± 0.005
593.6	$B\,^2\Sigma^+$	0	0.074 ± 0.005
594.0	$B\,^2\Sigma^+$	4	0.080 ± 0.005
594.7	$B\,^2\Sigma^+$	7	0.085 ± 0.010
595.3	$B\,^2\Sigma^+$	10	0.090 ± 0.010

$B\,^2\Sigma^+$–$X\,^2\Sigma^+$ bands, at 620.5 and 593.6 nm, respectively. Trace (a) corresponds to the peak of the $A\,^2\Pi_{3/2}$–$X\,^2\Sigma^+$ sub-band at 618.0 nm, while traces (b)–(d) are for the B-X band system and correspond to increasing vibrational excitation of the CaCl(B) product. Each trace required 512 sweeps (about 10 min.) using a resolution of 0.8 nm (full width at half-maximum). Notice that while the A-X signal reaches a maximum for perpendicular E vector alignment, that for all the B-X signals reach maxima for parallel alignment.

We quantify the alignment dependence in terms of a reagent alignment sensitivity factor S defined as

$$S = \frac{I(\mathbf{E}\parallel\bar{\mathbf{v}}_{rel}) - I(\mathbf{E}\perp\bar{\mathbf{v}}_{rel})}{I(\mathbf{E}\parallel\bar{\mathbf{v}}_{rel}) + I(\mathbf{E}\perp\bar{\mathbf{v}}_{rel})}\ , \tag{5}$$

where $I(\mathbf{E}\parallel\bar{\mathbf{v}}_{rel})$ and $I(\mathbf{E}\perp\bar{\mathbf{v}}_{rel})$ are intensities obtained with E parallel and perpendicular to the average relative velocity vector, respectively. S ranges from +1 where $I(\mathbf{E}\parallel\bar{\mathbf{v}}_{rel}) \gg I(\mathbf{E}\perp\bar{\mathbf{v}}_{rel})$ to −1 where $I(\mathbf{E}\parallel\bar{\mathbf{v}}_{rel}) \ll I(\mathbf{E}\perp\bar{\mathbf{v}}_{rel})$; when $S=0$, there is no alignment preference. Table I lists values of S for the four wavelengths reported here as well as those reported previously.[24] Also shown in Table I are estimates for the lower bound of the vibrational levels contributing to the chemiluminescence at the given wavelengths. These are estimated from Fortrat diagrams[36] constructed from known spectroscopic data.[37]

The variation of atomic calcium $^1S_0$–$^1P_1$ fluorescence with E vector alignment is shown in Fig. 8. This was recorded using the output of PM 2 (Sec. II B) and reveals a very high degree of polarization, indicated by $S = 0.950\pm0.005$, which is calculated allowing for the 45° angle between the viewing direction (PM 2) and $\bar{\mathbf{v}}_{rel}$.

3. Chemiluminescence polarization

The polarization of the product emission was measured using a photoelastic modulator (Hinds International, PEM 3) placed in front of the monochromator entrance slit.[38,39] This device consists of a vibrating calcium fluoride crystal which retards light by one half-wave at the point of peak compression and not at all at minimum compression. Thus together with a linear polarizer, it allows fluorescence polarization to be measured accurately. We define the degree of linear polarization P as

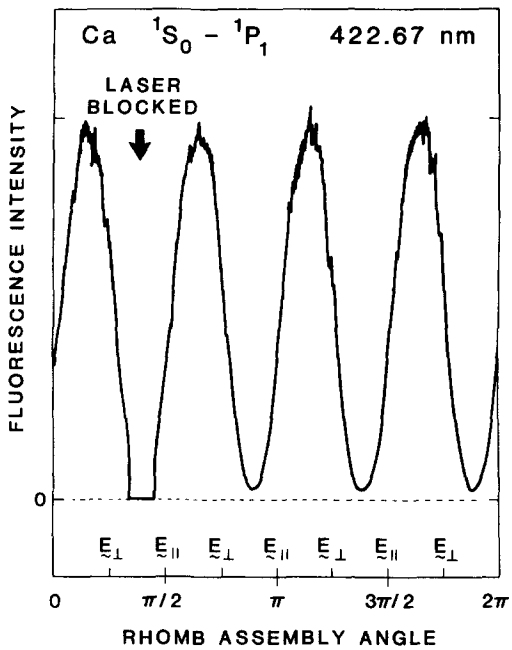

FIG. 8. Variation of the Ca $^1S_0$–$^1P_1$ fluorescence at 422.67 nm with rhomb assembly angle. Since signals were taken from PM 2, this response exhibits a $\pi/4$ phase difference from signals detected by PM 1.

$$P = \frac{I_\parallel - I_\perp}{I_\parallel + I_\perp} , \tag{6}$$

where $I_\parallel$ and $I_\perp$ are the fluorescence intensities passed by a polarizer held parallel and perpendicular to the atomic beam, respectively. In analogy to S, $-1 \le P \le +1$. For the peak of $\Delta v = 0$ sequence of the $B\,^2\Sigma^+$–$X\,^2\Sigma^+$ system we obtain $P = 0.20 \pm 0.01$, this value being independent, within the error bars, of the direction of the laser E vector.

4. Absolute chemiluminescence cross section

The absolute chemiluminescence cross section for this reaction was estimated by comparison of the chemiluminescence intensity with the Ca $^1S_0$–$^1P_1$ emission while spinning the laser E vector to minimize polarization effects. This ratio can be related to the branching for decay of the Ca($^1P_1$) state as shown by Dagdigian[40] and Telle and Brinkmann.[27] Radiative decay produces emission proportional to

$$I(\mathrm{Ca}^*) = n(\mathrm{Ca}\,^1P_1) A(^1S_0 - {}^1P_1) , \tag{7}$$

while the rate of excited CaCl production is proportional to the chemiluminescence cross section σ_{chem}:

$$I(\mathrm{CaCl}^*) = n(\mathrm{Ca}\,^1P_1)\, n(\mathrm{HCl})\, \sigma_{\mathrm{chem}}\, \bar{v}_{\mathrm{rel}} . \tag{8}$$

Here n(Ca $^1P_1$) and n(HCl) are the number densities of the reagents, $A(^1S_0$–$^1P_1)$ the radiative rate of the Ca $^1S_0$–$^1P_1$ transition and $\bar{v}_{\mathrm{rel}}$ the mean relative velocity. Thus,

$$\sigma_{\mathrm{chem}} = A(^1S_0 - {}^1P_1)\, I(\mathrm{CaCl}^*)/I(\mathrm{Ca}^*)\, n(\mathrm{HCl})\, \bar{v}_{\mathrm{rel}} . \tag{9}$$

Comparison of I(Ca*) and I(CaCl*) requires care since the atomic emission is orders of magnitude more intense. Using combinations of calibrated neutral density filters and correcting for the relative spectral response of the detection system we obtain $I(\mathrm{Ca}^*)/I(\mathrm{CaCl}^*) \simeq 10^4$, where I(Ca*) and I(CaCl*) refer to the relative spectral *areas*. Using the known[32] value of $A(^1S_0$–$^1P_1)$, the value of $\bar{v}_{\mathrm{rel}}$ estimated to be $\simeq 10^3$ ms^{-1} for an effusive Ca beam impinging on HCl gas,[28] and the value of n(HCl) measured with a calibrated ion gauge, we obtain

$$\sigma_{\mathrm{chem}} \simeq 68 \pm 15 \text{ Å}^2 \tag{10}$$

for the Ca($^1P_1$) + HCl reaction. This represents the total cross section for the production of visible emission and applies to an unpolarized excitation laser, since measurements were made with the laser E vector spinning. However, no allowance has been made for the spatial anisotropy of the fluorescence, but as most emission originates from the weakly polarized CaCl A–X system, this is likely to involve only a small error.

B. Ca($^1P_1$) + Cl_2

1. Chemiluminescence spectra

Figure 9(a) shows the laser-induced chemiluminescence spectrum obtained for this reaction. This was recorded under similar conditions to those for Fig. 5 except that a resolution of 0.8 nm was employed. The peak at 620.8 nm corresponds to $\sim 3\times10^2$ counts/s, which is about an order of magnitude less than for Ca($^1P_1$) + HCl at this resolution. This spectrum clearly indicates a much higher degree of rovibrational excitation for the CaCl* product than for the HCl reaction. Again, there is a rough similarity to a Ca metastable reaction, namely to Ca($^3P_{2,0}$) + Cl_2.[26,27] The most noticeable difference is the enhancement of the B–X $\Delta v = 0$ feature at 593.6 nm in the Ca($^1P_1$) case. However, the highly congested nature of these spectra prohibits a clear demarkation of A–X and B–X features. We estimate only an upper limit for the branching ratio between these two states. We estimate only an upper limit for the branching ratio between these two states. We find $\sigma(A)/\sigma(B) \gtrsim 6$. This compares with the ratio $\sigma(A)/\sigma(B) > 30$ for the reaction of Ca($^3P_{2,1,0}$) with Cl_2 given by Telle and Brinkmann.[27] A statistical partitioning of electronic energy based on Eq. (4) would predict $\sigma(A)/\sigma(B) \simeq 2.2$ for the Ca($^1P_1$) + Cl_2 reaction. Thus in contrast to the HCl reaction, a nonstatistical partitioning of electronic energy is suggested.

Unlike the HCl case, a weak chemiluminescence persists in the absence of Ca($^1P_1$) excitation, as shown in Fig. 9(b). Although this emission is at least two orders of magnitude less intense than the Ca($^1P_1$) + Cl_2 emission it is remarkably sharp, permitting a spectrum to be recorded. This emission, obtained with the laser off, varied both with Ca beam intensity and Cl_2 pressure. While it is possible to attribute this emission to a chemiluminescent reaction of metastable species present in the Ca beam, this seems unlikely since no analogous reaction is observed for either HCl or CCl_4. Figure 9(c) shows a spectrum obtained using a somewhat higher Ca beam intensity, corresponding to an oven temperature of 1175 K. [Recall that the requirement for the beam to be optically thin limits beam in-

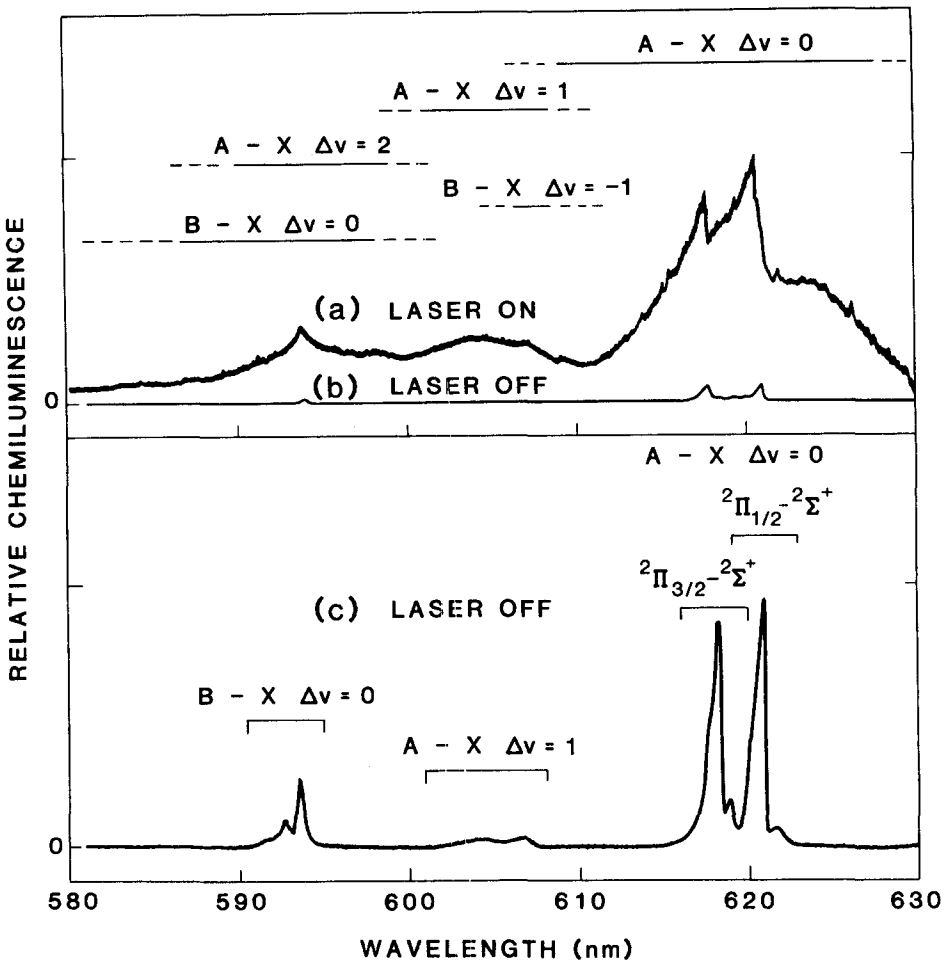

FIG. 9. Chemiluminescence spectrum (a) obtained by preparing Ca ($^1P_1$) in a beam impinging on Cl_2 gas; (b) obtained under the same conditions but with the laser blocked; and (c) obtained with a more intense calcium beam. While trace (a) corresponds to a high degree of rotational-vibrational excitation of the CaCl* product, traces (b) and (c) appear remarkably cold.

tensity for the Ca($^1P_1$) case]. The peak at 620.8 nm corresponds to 50 counts/s. Two possible causes for this emission are reaction of Cl_2 with Ca($^1S_0$) or with Ca_2. The first possibility is inconsistent with the most recent estimate[26] of D_0^0(CaCl) ~ 413 kJ/mol while the second possibility requires a four-center reaction. Whatever its source, the resulting CaCl A-X and B-X chemiluminescence is remarkably cold.

2. *Dependence on reagent alignment*

Rotation of the laser **E** vector reveals a strong alignment dependence for the Ca($^1P_1$) + Cl_2 chemiluminescent reaction, as illustrated in Fig. 10. It is immediately apparent that this system exhibits markedly different behavior from the reaction with HCl (Fig. 7). We see that the $A\,^2\Pi$–$X\,^2\Sigma^+$ transition at 620.8 nm displays the same phase dependence as the HCl case, namely, maximum for **E** perpendicular to $\bar{v}_{rel}$ but with a very much larger amplitude. Moreover, the signal observed at 593.6 nm corresponding to $B\,^2\Sigma^+$–$X\,^2\Sigma^+$ also shows the *same* alignment preference but with a smaller amplitude. Finally, notice that a small signal persists in the absence of Cl_2. This is caused by scattered light which becomes significant relative to the smaller signals obtained from the Ca($^1P_1$) + Cl_2 reaction. In estimating S, due allowance is made for this contribution. We obtain $S = -0.14 \pm 0.01$ for $\lambda = 620.8$ nm, and $S = -0.065 \pm 0.010$ for $\lambda = 593.6$ nm.

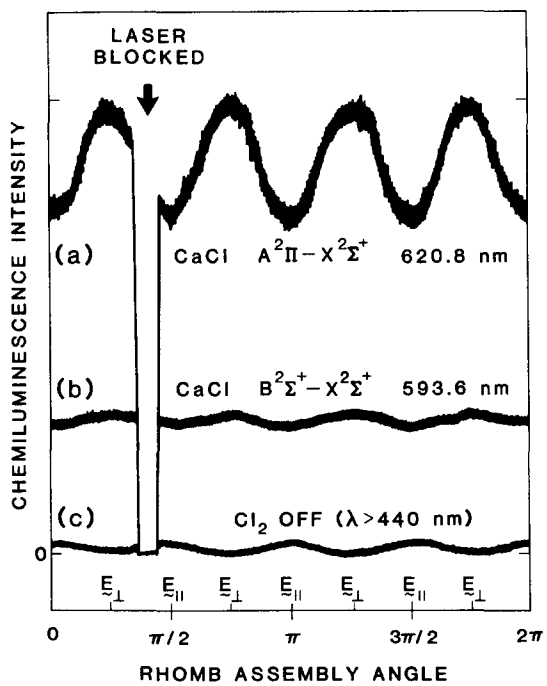

FIG. 10. Variation with rhomb assembly angle of chemiluminescence intensity from the reaction of Ca ($^1P_1$) with Cl_2. Trace (a) was recorded at the peak of the $A\,^2\Pi_{1/2}$–$X\,^2\Sigma^+$ system while trace (b) refers to the $B\,^2\Sigma^+$–$X\,^2\Sigma^+$ system. Trace (c), recorded in the absence of Cl_2 gas, is due to scattered light which varies with the direction of the laser **E** vector.

Measurements were also made at three other wavelengths 617.5, 605.0, and 587.5 nm. These correspond to the nominal positions of the $A\,^2\Pi_{3/2}-X\,^2\Sigma^+$ ($\Delta v=0$), $A\,^2\Pi_{3/2,1/2}-X\,^2\Sigma^+$ ($\Delta v=1$), and to both $B\,^2\Sigma^+-X\,^2\Sigma^+$ ($\Delta v=0$) and $A\,^2\Pi_{3/2,1/2}-X\,^2\Sigma^+$ ($\Delta v=2$) transitions, respectively [see Fig. 9]. The results are summarized in Table II.

3. Chemiluminescence polarization

We find no significant variation in polarization of the chemiluminescence with the direction of the laser E vector. Values obtained are $P=-0.002\pm0.002$ at 620.8 nm, $P=-0.03\pm0.01$ at 617.5 nm, and $P=0.08\pm0.02$ at 593.6 nm. In all cases a 1.0 nm resolution was employed.

4. Absolute chemiluminescence cross section

The absolute cross section for visible emission is measured exactly as described for the HCl case (Sec. III A 4). Allowing for the small contribution from the dark reaction, we obtain

$$\sigma_{\text{chem}} \simeq 20\pm7\ \text{Å}^2\ . \tag{11}$$

Again, this refers to the hypothetical case of an unpolarized laser, and no correction has been made for the fluorescence anisotropy. We note that this value is slightly lower ($\lesssim 5\%$) than that which would be obtained from a truly isotropic $Ca(^1P_1)$ orbital distribution; since laser excitation cannot prepare $Ca(^1P_1)$ orbitals aligned along the direction of propagation of the laser.

5. Chemi-ionization

As well as the above-mentioned chemiluminescence channels, a strong laser-induced chemi-ionization signal was observed in the case of Cl_2. We stress that chemi-ions could not be detected for either the HCl or CCl_4 cases. In addition a weak chemi-ion signal could be detected in the absence of the laser.

Typical ion currents were $\sim 10^{-9}$ A with the calcium beam, the Cl_2 gas at 3×10^{-4} Torr and with the laser tuned to the Ca $^1S_0-^1P_1$ line. In the absence of Cl_2, a current $\sim 10^{-10}$ A was obtained but only so long as the laser is tuned to the atomic line. Finally, with the laser blocked but with the calcium beam on and the Cl_2 present, a current of $\sim 2\times10^{-11}$ A resulted. The laser-induced chemi-ionization signal is found to increase linearly with the laser power. Removal of the etalon from the dye laser cavity caused the laser power to increase but the chemi-ion signal decreased in exact proportion to the Ca $^1S_0-^1P_1$ fluorescence. Switching the collection plate polarities caused an exact reversal of the chem-ionization current.

TABLE II. Reagent alignment sensitivity factors at various wavelengths for the chemiluminescent reaction Ca $(^1P_1)+Cl_2$.

λ (nm)	Nominal excited state	S
620.8	$A\,^2\Pi_{1/2}$ ($\Delta v=0$)	-0.140 ± 0.010
617.5	$A\,^2\Pi_{3/2}$ ($\Delta v=0$)	-0.145 ± 0.015
605.0	$A\,^2\Pi_{3/2,\,1/2}$ ($\Delta v=1$)	-0.150 ± 0.020
593.6	$B\,^2\Sigma^+$ ($\Delta v=0$)	-0.065 ± 0.010
587.5	$B\,^2\Sigma^+$ ($\Delta v=0$)	-0.090 ± 0.015
	$A\,^2\Pi_{3/2,\,1/2}$ ($\Delta v=0$)	

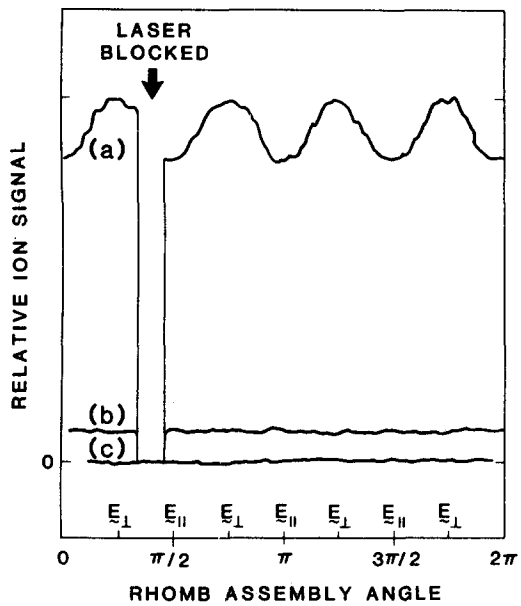

FIG. 11. Variation with rhomb assembly angle of chemi-ionization signals from the reaction of Ca $(^1P_1)$ with Cl_2; trace (a), taken with the laser tuned to the Ca $^1S_0-^1P_1$ transition in the presence of Cl_2 gas. Trace (b) is obtained under the same conditions as trace (a) but with the Cl_2 gas turned off. Trace (c) displays the baseline obtained with the laser turned off the Ca line.

Examination of the $Ca(^1P_1)$ alignment dependence of this channel revealed a moderate E vector dependence. This is illustrated in Fig. 11. Analysis of the data yields $S=-0.095\pm0.005$ for the $Ca(^1P_1)+Cl_2$ chemi-ionization channel.

C. $Ca(^1P_1)+CCl_4$

Laser-induced chemiluminescence signal levels at 593.6 and 620.8 nm were found to be of the same order as those from the Cl_2 reaction. No chemiluminescence spectrum was recorded but we note that a factor of 2.5 times more signal is obtained at 620.8 nm than at 593.6 nm. We estimate a branching ratio of $\sigma(A)/\sigma(B)=4.0\pm1.5$ for this reaction.

Our primary interest with this system was in examining the dependence of the chemiluminescence on $Ca(^1P_1)$ alignment. For both wavelengths, only a very weak indication of any reactive asymmetry could be detected. At 593.6 nm we found $S=0.015\pm0.010$ while at 620.8 nm, $S=0.02\pm0.01$.

An absolute chemiluminescence cross section is estimated to be

$$\sigma_{\text{chem}}=8^{+5}_{-3}\ \text{Å}^2\ . \tag{12}$$

For reference purposes, we collect in Table III the ab-

TABLE III. Absolute chemiluminsecence cross sections and branching ratios.

Reagents	σ_{chem} (Å^2)	$\sigma(A)/\sigma(B)$
Ca ($^1P_1$) + HCl	68 ± 15	2.5 ± 0.1
Ca ($^1D_2$) + HCl	25 ± 5[a]	4.4 ± 0.2 4.0 ± 1.0[a]
Ca ($^1P_1$) + Cl_2	20 ± 7	$\gtrsim 6$
Ca ($^1P_1$) + CCl_4	8^{+5}_{-3}	4.0 ± 1.0

[a]Reference 27.

solute chemiluminescence cross sections and branching ratios for the reactions considered in this study.

IV. DISCUSSION

A. General remarks

We have studied the dependence on Ca p-orbital alignment of the laser-induced chemiluminescent reaction of Ca($^1P_1$) with HCl, Cl_2, and CCl_4, as well as the laser-induced chemi-ionization reaction of Ca($^1P_1$) with Cl_2. Table IV summarizes our results in terms of the alignment sensitivity factor S. Whereas Ca($^1P_1$) + HCl and Ca($^1P_1$) + Cl_2 both show substantial sensitivity to th alignment of the Ca p orbital, the Ca($^1P_1$) + CCl_4 reaction is almost independent of such alignment. This ia an important negative result. Although its interpretation is unclear at present, there are many reasons for expecting such behavior, e.g., the possibility of complex formation, the multiplicity of available Cl atoms at different angles to the approach direction, etc.

Before considering in detail the Ca($^1P_1$) + HCl and Ca($^1P_1$) + Cl_2 reaction systems, we note that we have controlled only a single aspect of the overall collision geometry, namely, that of the Ca p-orbital approach direction. Consequently, our observations refer to an average over all impact parameters and an average over the spatial distribution of the other reaction partner. Furthermore, even the p-orbital alignment is imperfect because of the spread in initial relative velocity vectors implicit in a beam-gas scattering geometry. Although the most probable initial relative velocity vector $\mathbf{v}_{rel}$ lies along the beam axis z, there exists a distribution in relative velocity vector directions due to the addition of the (small) randomly oriented velocity of the collision partner to that of the Ca($^1P_1$) atom directed along the beam axis. We estimate[28] values for $\langle\cos^2\theta\rangle$ where θ is the angle between $\mathbf{v}_{rel}$ and z. For Ca + HCl, $\langle\cos^2\theta\rangle \simeq 0.80$; for Ca + Cl_2, $\langle\cos^2\theta\rangle \simeq 0.90$; and for Ca + CCl_4, $\langle\cos^2\theta\rangle \simeq 0.93$. Although somewhat stronger alignment effects would be expected under ideal crossed beam conditions ($\langle\cos^2\theta\rangle = 1$), the beam-gas collision geometry does not seriously impair the ability to make vector measurements, as stressed previously.[28]

It may be wondered whether the observed sensitivity factors indeed refer to the reaction rates of various product channels or if they represent instead changes in the chemiluminescence intensity in the direction of the detector caused by changes in the *spatial* distribution (or polarization) of the emission. From the available evidence, we deduce that the observed effects are predominantly due to the first possibility. Let us consider in turn the reactions of Ca($^1P_1$) with Cl_2 and HCl. The system Ca($^1P_1$) + Cl_2 – CaCl($A\,^2\Pi$) + Cl produces essentially unpolarized emission, yet this provides the largest variation of signal with Ca p-orbital alignment. Furthermore, the chemiluminescence results are in accord with the chemi-ionization channel of this reaction, for which there is no ambiguity since all product ions are collected. Thus, for this case, it seems clear that product polarization effects are dominated by the variation of reaction rates with approach geometry.

The Ca($^1P_1$) + HCl results might be regarded as more ambiguous because this reaction produces highly polarized products as a consequence of kinematic constraints.[41–44] In this reaction the orbital angular momentum of the reagents is large compared to one unit of $\hbar$, i.e., the Ca($^1P_1$) contribution. Under these conditions, polarization effects alone cannot account for S, i.e., nonzero values of S imply that the reaction rates depend on alignment. Moreover, so long as there is cylindrical symmetry of the Ca p orbital about the other reagent, only variations in reaction rates can contribute to S. Actually, the cylindrical symmetry is broken when the Ca p orbital is aligned perpendicular to its flight direction. However, if there is orbital following, in which the symmetry of the electronic state remains unchanged as the reagents approach (see Sec. IV D), the cylindrical symmetry is effectively restored. We believe this to be the case.

As a further check, the CaCl* product polarization was measured for the Ca p orbital aligned parallel and perpendicular to its flight direction. The values of P were found to be the same within the experimental error. Thus in what follows we interpret S as arising only from the variation of reaction rate with reagent approach geometry.

B. Interpretation of Ca($^1P_1$) + HCl alignment dependence

We have shown that alignment of the Ca p orbital perpendicular to the direction of approach enhances production of the CaCl($A\,^2\Pi$) state while the CaCl($B\,^2\Sigma^+$) state product is favored by parallel approach. Knowing the branching ratio between these two states $\sigma(A)/\sigma(B) \simeq 2.5$, we determine the dependence of the total chemiluminescence cross section on p-orbital alignment. We find that this quantity

$$S_{A,B} = S_A(\sigma_A/\sigma_B) + S_B\,, \tag{13}$$

TABLE IV. Average values of the reagent sensitivity factor S.[a]

	Products		
Reagents	CaCl ($A\,^2\Pi_{1/2}$) + X	CaCl ($B\,^2\Sigma^+$) + X	$CaCl^+ + X^-$
Ca ($^1P_1$) + HCl	−0.034 ± 0.005	0.080 ± 0.005	...
Ca ($^1P_1$) + Cl_2	−0.140 ± 0.010	−0.065 ± 0.010	−0.095 ± 0.005
Ca ($^1P_1$) + CCl_4	0.020 ± 0.010	0.015 ± 0.010	...

[a]Defined in Eq. (5).

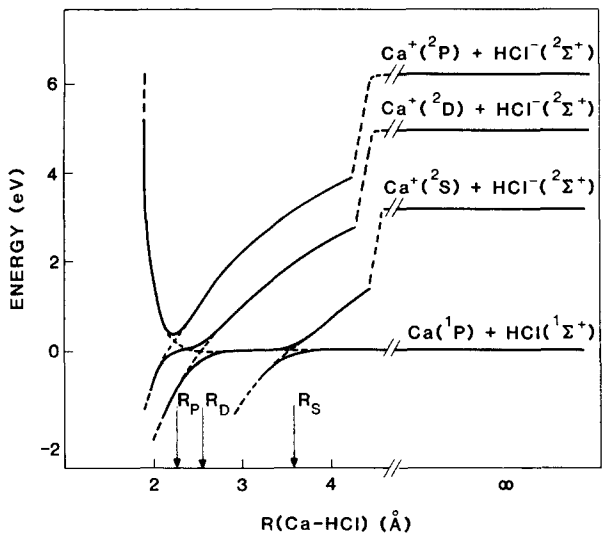

FIG. 12. Schematic diagram of the potential curves appropriate to the electron-jump model of the Ca($^1P_1$) + HCl reaction. The covalent Ca($^1P_1$) + HCl ($^1\Sigma^+$) surface is crossed by three ionic surfaces. These crossings occur at R_S, R_D, and R_P, corresponding to formation of HCl^- ($^2\Sigma^+$) with the ^2S, ^2D, and ^2P states of the Ca^+ ion, respectively. Other covalent curves, e.g., Ca ($^1D_2$) + HCl, have been omitted for clarity.

is essentially invariant with the alignment, i.e., $S_{A,B} = 0.00 \pm 0.01$.

We believe that these results can be qualitatively rationalized in terms of a simple molecular orbital picture, involving an electron-jump "harpoon" mechanism.[44] The large value of the chemiluminescence cross section (68 ± 15 Å^2) is certainly indicative of an electron-jump mechanism. Here an electron is transfered from the Ca($^1P_1$) atom to the HCl molecule as the reagents approach. This transfer is considered to occur at a point where the covalent Ca($^1P_1$) + HCl surface crosses an ionic $Ca^+ + HCl^-$ surface of the same symmetry. Figure 12 displays a schematic representation of the relevant curves for the Ca($^1P_1$) + HCl system.

Three ionic surfaces are included, corresponding to production of the ^2S, ^2D, and ^2P states of the Ca^+ ion, together with the $^2\Sigma$ state of the HCl^- ion. For simplicity, only the Ca($^1P_1$) + HCl($^1\Sigma^+$) covalent surface is shown. Three crossing points are indicated, occurring at distances R_S, R_D, and R_P, obtained by equating the (Coulomb) energy released by ion pair formation with the energy difference between the ionic and covalent states. Using a value of -0.8 eV[44] for the vertical electron affinity of HCl, we find $R_S = 3.6$, $R_D = 2.5$, and $R_P \simeq 2.2$ Å, its precise value being dependent on the form of the Ca($^1P_1$) + HCl($^1\Sigma^+$) short range potential.

In principle, the electron jump may occur at any of these points. However, the longer range of the R_S crossing makes this the most likely location. Here the Ca p-orbital electron is transferred to HCl, producing an HCl^-($^2\Sigma^+$) ion which rapidly dissociates, forming $Ca^+Cl^- + H$. The large amount of energy released permits population of both the $A\,^2\Pi$ and $B\,^2\Sigma^+$ states as well as the ground $X\,^2\Sigma^+$ state of CaCl.

The electron jump need not occur with unit probability at R_S, permitting the system to access R_D and R_P. The symmetry of the Ca + HCl system is such that both ionic and covalent states will, in general, possess a sole symmetry element, that of the reaction plane, irrespective of the p-orbital alignment. Thus it is unlikely that orbital alignment will affect the probability of an electron jump at R_S. Moreover, having jumped, the prior alignment of the Ca($^1P_1$) electron becomes irrelevant. Hence we look to the inner crossings, in which an s electron may jump leaving an aligned ionic Ca orbital, as the source of the observed alignment dependence. In this case we propose that the p orbital of the Ca atom transforms into a CaCl molecular orbital and that its alignment serves to differentiate between the $A\,^2\Pi$ and $B\,^2\Sigma^+$ electronic states. Indeed, these states are known to possess a high degree of Ca^+ $4p$ and $3d$ character,[45] the excited electron being localized on the Ca^+ ion. In particular, the highest occupied π molecular orbital of the Ca(A) state may be considered to arise largely from an hydridization of the Ca^+ $4p\pi$ and $3d\pi$ nonbonding orbitals, whereas the analogous σ molecular orbital of the Ca(B) state arises from hybrized Ca^+ $4p\sigma$ and $3d\sigma$ orbitals. Thus, perpendicular (π) alignment of the Ca($^1P_1$) orbital leads to enhancement of the CaCl ($A\,^2\Pi$) state product built up from the Ca^+ $4p\pi/3d\pi$ molecular orbitals, while parallel (σ) alignment enhances the CaCl($B\,^2\Sigma^+$) product built up from the Ca^+ $4p\sigma/3d\sigma$ orbitals.

The relatively small magnitude of the alignment dependence of the $A\,^2\Pi/B\,^2\Sigma^+$ branching is consistent with the reaction occurring largely by way of an electron jump at R_S, in which case excited CaCl states are produced without regard for the Ca($^1P_1$) alignment. The close agreement between the observed $\sigma(A)/\sigma(B)$ branching ratio and the statistical prediction is further support for this contention.

Recall that within a given A-X or B-X band system, the chemiluminescence at different wavelengths displayed a similar dependence on the orbital alignment (Table I). In the case of the B-X system, a very slight increase in S is perceptible as the chemiluminescence wavelength increases, corresponding to higher vibrational excitation of the CaCl($B\,^2\Sigma^+$) product. Although the variation observed here is barely statistically meaningful, further comment is merited in order to illustrate the importance of such observations. Conservation of the total angular momentum and energy of the system requires that the impact parameter of the reaction decreases for production of the more highly vibrationally excited products. This is best illustrated by considering the limiting case when all the available energy of the system appears as vibration. Then none is left for rotation, a situation that is only possible for an initial impact parameter b of zero. In this way, study of high vibrational states might be regarded as analogous to examining the back-scattered products in angular distribution measurements.[4,12] The slight effect observed here, if real, is consistent with the accessibility of the inner crossing point for small impact parameters, contrasted with the inaccessibility for impact parameters significantly greater than R_D, R_P.

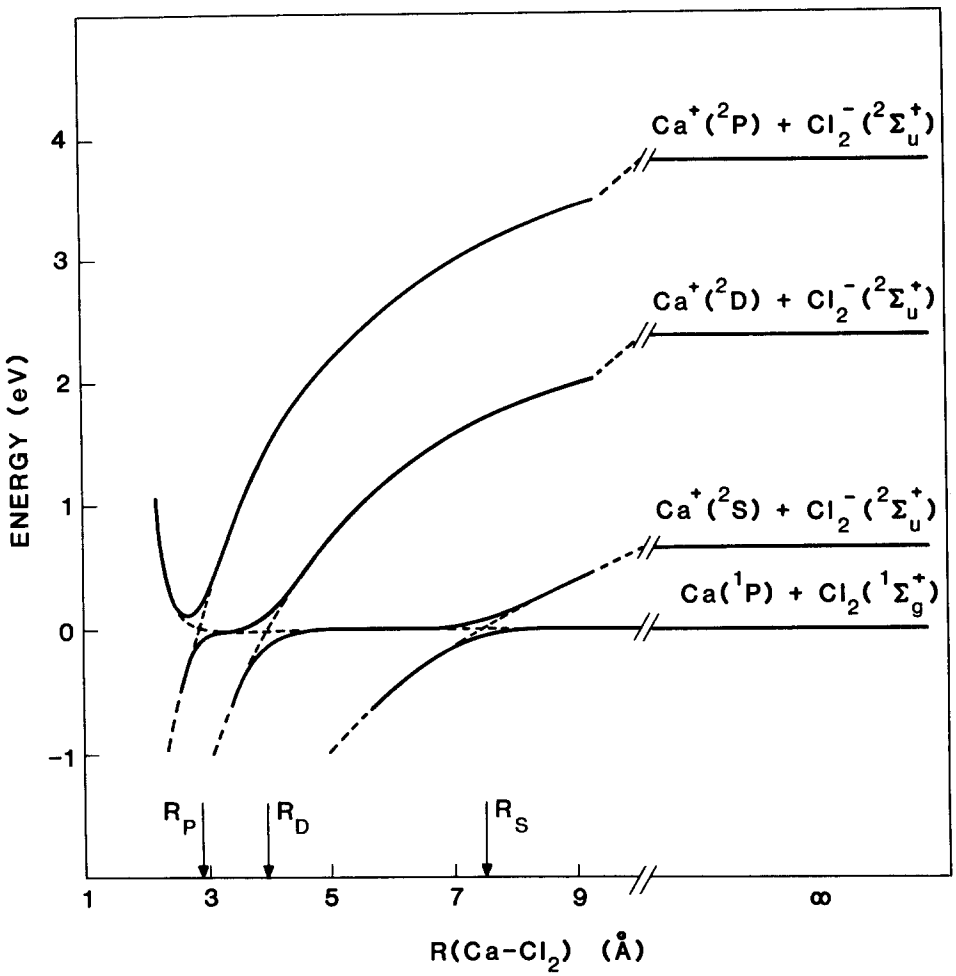

FIG. 13. Schematic diagram of the potential curves appropriate to the electron-jump model of the Ca $(^1P_1) + Cl_2$ reaction. The Ca $(^1P_1) + Cl_2$ covalent surface is crossed by three ionic surfaces. These crossings occur at R_S, R_D, and R_P, corresponding to formation of Cl_2^- $(^2\Sigma_u^+)$ with the ^2S, ^2D, and ^2P states of Ca^+, respectively. Other covalent curves, e.g., Ca $(^1D_2) + Cl_2$, have been omitted for clarity.

C. Interpretation of Ca$(^1P_1)$ + Cl_2 alignment dependence

Both the CaCl$(A\,^2\Pi)$ and $(B\,^2\Sigma^+)$ products are enhanced by perpendicular (π) p-orbital alignment, as is the chemi-ionization channel. However, each of these processes exhibits a quantitatively different dependence, the CaCl$(A\,^2\Pi)$ product displaying the largest effect.

Again an electron-jump model serves to rationalize these findings. Figure 13 shows a schematic representation of the relevant covalent $Ca(^1P_1) + Cl_2(^1\Sigma_g^+)$ and ionic $Ca^+(^2S, ^2D, ^2P) + Cl_2^-(^2\Sigma_u^+)$ potentials. In this case, we have employed a vertical electron affinity for Cl_2 of 1.3 eV.[46] The arguments concerning production of CaCl excited states parallel those presented for the HCl reaction but with one important difference, namely, the increased symmetry of the system results in an alignment dependence of the electron jump at R_S. The symmetry of the various three-atom states for the covalent $Ca(^1P_1) + Cl_2(^1\Sigma_g^+)$ and ionic $Ca^+(^2S_0) + Cl_2^-(^2\Sigma_u^+)$ systems are indicated in Table V. Here we consider only the limiting cases of collinear ($C_{\infty v}$) and "broadside" (C_{2v}) collision. An avoided crossing is expected when covalent and ionic states possess the same symmetry. Let the magnitude of the splitting be denoted by ΔV. An electron jump occurs if ΔV is sufficiently large to ensure that the system remains on the same adiabatic surface. For geometries intermediate between those considered in Table V, smaller splittings are expected, typically scaling with the square of the sine or cosine of the angle included by the three atoms.[48] Thus the enhancement of the total chemiluminescence cross section by perpendicular approach is indicative that broadside attack is favored.

Taking our estimate for the $\sigma(A)/\sigma(B)$ ratio together with the S values of the individual channels, we find that $S_{A,B} = -0.135 \pm 0.015$ for the total chemiluminescence cross section, compared to the total chemi-ionization cross section for which $S = -0.095 \pm 0.005$. Thus, the ionic channel displays a somewhat reduced dependence on Ca p-orbital alignment compared to either the CaCl$(A\,^2\Pi)$ channel or the total chemiluminescence sig-

TABLE V. Correlations of potential energy surfaces.[a]

System		Collinear $C_{\infty v}$	Broadside C_{2v}
Covalent:	Ca $^1P\sigma$ + Cl_2 $(^1\Sigma_g^+)$	$^1\Sigma^+$	$^1A_1$
	Ca $^1P\pi$ + Cl_2 $(^1\Sigma_g^+)$	$^1\Pi^+$	$^1B_1$
	Ca $^1P\pi$ + Cl_2 $(^1\Sigma_g^+)$	$^1\Pi^-$	$^1B_2$
Ionic	$Ca^+(^2S) + Cl_2^-(^2\Sigma_u^+)$	$^1\Sigma^+$	$^1B_1$

[a]The notation is identical to that employed in Ref. 47. The molecule lies in the xz plane.

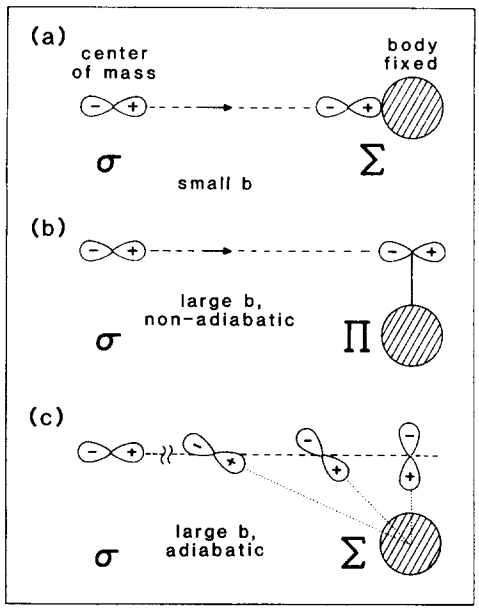

FIG. 14. Relationship between the center-of-mass and body-fixed frames. At small impact parameters, parallel center-of-mass alignment, denoted by σ, transforms to parallel body-fixed alignment, denoted by Σ. At large impact parameters, parallel center-of-mass alignment can give rise to perpendicular Π body-fixed alignment for nonadiabatic behavior, or to Σ alignment if "orbital following" occurs, as in adiabatic behavior.

nal, but a greater effect than the $CaCl(B\,^2\Sigma^+)$ channel. This is consistent with the fact that the $CaCl(B\,^2\Sigma^+)$ state has a slightly lower ionization potential than the $CaCl(A\,^2\Pi)$ state, making formation of $CaCl^+ + Cl^-$ more likely through the σ configuration.

Finally, we notice that if the dependence of the *total* chemiluminescence cross section on p-orbital alignment $S_{A,B} \simeq -0.135$ is subtracted from the values for the individual channels ($S_A \simeq -0.145$, $S_B \simeq -0.065$) we obtain $S'_A \simeq -0.01 \pm 0.02$ and $S'_B \simeq +0.07 \pm 0.02$. These S values are of the same order and sign as for the HCl case. This supports the contention that the primary difference between these two reactions is that the *total* chemiluminescence cross section is dependent on the p-orbital alignment in the Cl_2 case but not for the HCl reaction. Thus the electron-jump model provides a unifying framework for describing the observed reactive asymmetries with atomic reagent alignment.

D. Relation between center-of-mass and body-fixed alignment

We have already mentioned that the laboratory alignment of the Ca p orbital is somewhat "smeared" in the center-of-mass (c.m.) frame due to the spread of scattering gas velocities. This is a small effect and should not invalidate any of the above deductions. However, a given c.m. alignment need not, *a priori*, be preserved in the *body-fixed* frame. Thus it is possible to picture an alignment of the p orbital parallel to the direction of approach in the c.m. frame, σ alignment, giving rise to either parallel Σ or perpendicular Π alignment in the body-fixed frame, depending on the impact parameter and the reagent interaction energy.[49] This behavior is illustrated in Fig. 14. In order for the system to switch from σ to Π alignment, Fig. 14(b), a nonadiabatic transition is required, at which point Ω (the projection of the electronic orbital angular momentum on the body-fixed axis) changes from 0 to 1. If this were indeed happening for the systems studied, we would not expect the direct correlations observed between σ and π reagent alignments and Σ and Π product channels. Thus, we believe that the system remains adiabatic $\Delta\Omega = 0$ as the reagents approach. This situation is illustrated in Fig. 14(c). Such an "orbital following" picture has been considered previously by Hertel[50] and has recently been tested by a number of studies in which aligned $Na(^2P_{3/2})$ atoms have been collided with $Na(^2P_{3/2})$[51] and $Hg(^1S_0)$[52,53] atoms as well as $Na^+(^1S_0)$ ions.[54] In addition, aligned $Ne(^3D_3)$ and $Ne(^3P_2)$ have been scattered from $Hg(^1S_0)$.[55] Adiabatic behavior is indicated in all cases. Although the exchange reactions examined here represent considerably more complex systems (for example, the target molecule rotates as the p orbital approaches) the same picture appears to be valid. Noting that the alignment dependence of the various reactive channels is not total, we cannot rule out contributions from nonadiabatic approach but we believe the reactive trajectories are predominantly adiabatic.

ACKNOWLEDGMENTS

We thank J. A. Guest and K. H. Jackson for assistance with the photoelastic modulator polarimeter. R. N. Z. gratefully acknowledges support through the Shell Distinguished Chairs program, funded by the Shell Companies Foundation, Inc. This work is supported by the National Science Foundation under grant NSF CHE 80-06524 and by the Air Force Office of Scientific Research under AFOSR 81-0053.

[1] K. J. Laidler, *Chemical Kinetics* (McGraw–Hill, New York, 1965); I. W. M. Smith, *Kinetics and Dynamics of Elementary Gas Reactions* (Butterworths, London, 1980).
[2] K. Fukui, T. Yonezawa, and H. Shingu, J. Chem. Phys. 20, 722 (1952); K. Fukui, T. Yonezawa, C. Nagata, and H. Shingu, *ibid.* 22, 1433 (1954).
[3] R. B. Woodward and R. Hoffmann, *The Conservation of Orbital Symmetry* (Chemie, Weinheim, 1970).
[4] See P. R. Brooks, Science 193, 11 (1976).
[5] P. R. Brooks and E. M. Jones, J. Chem. Phys. 45, 3449 (1966).
[6] P. R. Brooks, E. M. Jones, and K. Smith, J. Chem. Phys. 51, 3073 (1969).
[7] G. Marcellin, and P. R. Brooks, J. Am. Chem. Soc. 95, 7885 (1973); 97, 1710 (1975).
[8] K. H. Kramer and R. B. Bernstein, J. Chem. Phys. 42, 767 (1965).
[9] R. J. Beuhler, Jr., R. B. Bernstein, and K. H. Kramer, J. Am. Chem. Soc. 88, 5331 (1966).
[10] R. J. Beuhler, Jr. and R. B. Bernstein, Chem. Phys. Lett. 2, 166 (1968); 3, 118 (1969).
[11] R. J. Beuhler and R. B. Bernstein, J. Chem. Phys. 51, 5305 (1969).
[12] D. H. Parker, K. K. Chakravorty, and R. B. Bernstein, J. Phys. Chem. 85, 466 (1981); Chem. Phys. Lett. 86, 113 (1982).
[13] P. R. Brooks, J. Chem. Phys. 50, 5031 (1969).

[14]P. R. Brooks, J. S. McKillop, and H. G. Pippin, Chem. Phys. Lett. **66**, 144 (1979).
[15]D. van den Ende and S. Stolte, Chem. Phys. Lett. **76**, 13 (1980).
[16]A. Kastler, J. Phys. Radium **11**, 225 (1950).
[17]R. E. Drullinger and R. N. Zare, J. Chem. Phys. **51**, 5532 (1969); **59**, 4225 (1973).
[18]H. G. Dehmelt and K. B. Jefferts, Phys. Rev. **125**, 1318 (1962); K. B. Jefferts, Phys. Rev. Lett. **20**, 39 (1968); C. B. Richardson, K. B. Jefferts, and H. G. Dehmelt, Phys. Rev. **165**, 80 (1968); **170**, 350 (1968).
[19]J. H. Ling and K. R. Wilson, J. Chem. Phys. **65**, 881 (1976).
[20]R. N. Zare, Ber. Bunsenges Ges. **86**, 422 (1982).
[21]R. C. Estler and R. N. Zare, J. Am. Chem. Soc. **100**, 1323 (1978). Subsequent work shows that the I_2 + In, Tl ground state reactions were being observed, see Ref. 25.
[22]E. W. Rothe, F. Ranjbar, and D. Sinha, Chem. Phys. Lett. **78**, 16 (1981); **81**, 175 (1981).
[23]Z. Karny, R. C. Estler, and R. N. Zare, J. Chem. Phys. **69**, 5199 (1978).
[24]C. T. Rettner and R. N. Zare, J. Chem. Phys. **75**, 3636 (1981).
[25]C. T. Rettner, L. Wöste, and R. N. Zare, Chem. Phys. **58**, 371 (1981).
[26]U. Brinkmann and H. Telle, J. Phys. B **10**, 133 (1977).
[27]H. Telle and U. Brinkmann, Mol. Phys. **39**, 361 (1980); U. Brinkmann, V. H. Schmidt, and H. Telle, Chem. Phys. Lett. **73**, 530 (1980).
[28]M. G. Prisant, C. T. Rettner, and R. N. Zare, J. Chem. Phys. **75**, 2222 (1981).
[29]C. R. Webster, L. Wöste, and R. N. Zare, Opt. Commun. **35**, 435 (1980).
[30]R. L. Kohn, C. V. Shank, E. P. Ippen, and A. Dienes, Opt. Commun. **3**, 177 (1971).
[31]R. N. Diffenderfer, P. J. Dagdigian, and D. R. Yarkony, J. Phys. B **14**, 21 (1981).
[32]W. L. Wiese, M. W. Smith, and B. M. Miles, *Atomic Transition Probabilities* (U.S. GPO, Washington, D.C., 1969), Vol. II, p. 248.
[33]U. Dinur, R. Kosloff, R. D. Levine, and M. J. Berry, Chem. Phys. Lett. **34**, 199 (1975).
[34]M. B. Faist and R. D. Levine, Chem. Phys. Lett. **47**, 5 (1977).
[35]P. J. Dagdigian, H. W. Cruse, and R. N. Zare, J. Chem. Phys. **60**, 2330 (1974).
[36]M. G. Prisant (private communication).
[37]L. E. Berg, L. Klynning, and H. Martin, Phys. Scr. **22**, 216 (1980).
[38]K. H. Jackson, Ph.D. thesis, Stanford University, Stanford, California, 1981.
[39]M. G. Prisant, C. T. Rettner, and R. N. Zare, Chem. Phys. Lett. **88**, 271 (1982).
[40]P. J. Dagdigian, Chem. Phys. Lett. **55**, 239 (1978).
[41]D. S. Hsu, N. D. Weinstein, and D. R. Herschbach, Mol. Phys. **29**, 257 (1975).
[42]N. H. Hijazi and J. C. Polanyi, Chem. Phys. **11**, 1 (1975).
[43]D. R. Herschbach, Discuss. Faraday Soc. **33**, 283 (1962).
[44]D. R. Herschbach, Adv. Chem. Phys. **10**, 319 (1966).
[45]L. Klynning and H. Martin, Phys. Scr. **24**, 25, 33, (1981).
[46]R. Grice and D. R. Herschbach, Mol. Phys. **27**, 159 (1974).
[47]G. Herzberg, *Electronic Spectra and Electronic Structure of Polyatomic Molecules* (Van Nostrand Reinhold, New York, 1966).
[48]E. A. Gislason and J. G. Sachs, J. Chem. Phys. **62**, 2678 (1975).
[49]J. Grosser, J. Phys. B **14**, 1449 (1981).
[50]I. V. Hertel, Adv. Chem. Phys. **45**, 341 (1981).
[51]J. G. Kircz, R. Morgenstern, and G. Hienhuis, Phys. Rev. Lett. **48**, 610 (1981).
[52]L. Hüwel, J. Maier, R. K. B. Helbing, and H. Pauly, Chem. Phys. Lett. **74**, 459 (1980).
[53]L. Hüwel, J. Maier, and H. Pauly, J. Chem. Phys. **76**, 4961 (1982).
[54]H. Schmidt, A. Bähring, E. Meyer, and B. Miller (to be published).
[55]W. Bussert, J. Ganz, H. Hotop, M.-W. Ruf, A. Siegel, and H. Waibel, in *Proceedings XII ICPEAC, Abstracts of Contributed Papers*, edited by S. Datz (North-Holland, Amsterdam, 1981), p. 522.